



Contents lists available at ScienceDirect

Arabian Journal of Chemistry

journal homepage: www.ksu.edu.sa

Electrodeposited zinc oxide nanoparticles: Synthesis, characterization, and anti-cervical cancer effects

Yingying Chen^{a,b,c,1}, Xinxin You^{b,c,1}, Liya Ye^{b,c}, Shuangshuang Mei^{b,c}, Junhui Yu^{b,c}, Youyou Xie^d, Kai Wang^{b,c}, Xing Chen^{b,c,*}

^a Department of Gynaecology and Obstetrics, Women's Hospital, School of Medicine, Zhejiang University, Hangzhou, China

^b Department of Gynaecology and Obstetrics, Zhejiang University Affiliated Zhejiang Taizhou Hospital, Taizhou, China

^c Zhejiang Provincial Clinical Research Center for Obstetrics and Gynecology, Hangzhou, China

^d Department of radiotherapy, Zhejiang University Affiliated Zhejiang Taizhou Hospital, Taizhou, China

ARTICLE INFO

Keywords:

Zinc oxide
Nanoparticle
Electrodeposition
Anticancer
Cervical
Mechanism

ABSTRACT

In the present study, zinc oxide nanoparticles (ZnO NPs) were synthesized via the electrodeposition method and characterized. Then, the anticancer effects of ZnO NPs against cervical cancer HeLa cells were assessed by cell viability, oxidative stress, caspase activity, qRT-PCR, MMP, and ELISA assays. XRD analysis revealed the hexagonal wurtzite phase of ZnO. SEM image of ZnO NPs showed the homogeneous spherical/hexagonal-like structures of ZnO NPs, while TEM imaging revealed the successful synthesis of ZnO NPs with an average diameter of about 8 nm. The UV-vis absorption spectrum of ZnO NPs showed a characteristic absorption band around the wavelength of 368 nm with a band gap energy (E_g) of 3.36 eV. DLS study displayed that the obtained particle size of ZnO NPs has an average size of 29.24 nm and an average zeta potential value of -19 mV. Additionally, cellular findings indicated that the proliferation of cervical cancer HeLa cells was markedly mitigated after incubation with ZnO NPs at different concentrations of 10, 50 and 100 $\mu\text{g/ml}$, however, these concentrations were not able to trigger an apparent cytotoxic effect on HUVEC non-malignant cells. Also, it was detected that ZnO NPs led to overexpression of Bax/ Bcl-2, caspase-9/-3 genes, increased level of caspase-9/-3 activity, overproduction of MDA level, inhibition of SOD and CAT activity and reduction of GSH content, MMP collapse, and upregulation of cytoplasmic cytochrome c release. In general, these findings suggested that electrodeposited synthesized ZnO NPs can induce anticancer effects in cervical cancer HeLa cells through the mitochondrial-mediated apoptosis signaling pathway.

1. Introduction

Cancer is an abnormal process causing uncontrolled cell division which results in body tissue damage. A huge number of cancer cells have been studied so far to explore deeply their cellular and molecular characteristics and therapeutic responses. Cervical cancer is diagnosed in over 500,000 women worldwide each year, and over 300,000 women die from the disorder (Cohen et al., 2019). According to reports cervical malignancy acts as the second most common cancer among women worldwide (Movva et al., 2009). Most of the time, high-risk subtypes of the human papilloma virus (HPV) are the primary cause of cervical cancer. In low- and middle-income nations without routine screening or HPV vaccination plans, about 90 % of cervical cancer cases reported

(Cohen et al., 2019). The three main cancer therapies are radiotherapy, chemotherapy, and surgery; however, the main side effects of these approaches are low monitoring and accumulation of drugs in off-targeted tissues (Movva et al., 2009, Shanmugam et al., 2023, Varlotta and Cardarelli 2023). Therefore, failure of conventional therapeutic approaches can be appointed as an exceedingly discouraging experience (Burmeister et al., 2022). It is therefore important to find alternative therapeutic targets and potential chemotherapeutics to promote the anticancer potency of conventional treatment modalities while reducing the adverse effects (Kissel et al., 2020).

Nanoparticles (NPs) are the newest trending area of nanomedicine used in the manipulation of cancer therapy (Wolfram and Ferrari 2019, Giri et al., 2023). Because of their unique structural properties, NPs

* Corresponding author at: No.150, Ximen Street, Linhai 317000, China.

E-mail address: chenxing@enzemed.com (X. Chen).

¹ Same contribution.

<https://doi.org/10.1016/j.arabjc.2024.105992>

Received 25 July 2024; Accepted 12 September 2024

Available online 15 September 2024

1878-5352/Crown Copyright © 2024 Published by Elsevier B.V. on behalf of King Saud University. This is an open access article under the CC BY-NC-ND license (<http://creativecommons.org/licenses/by-nc-nd/4.0/>).

serve as great candidates to target the abnormal cell proliferation prompted by cancer (Pugazhendhi et al., 2018). NPs could effectively target the cancer cells leading to DNA damage and inducing genotoxicity (Naser et al., 2023).

Zinc oxide (ZnO) NPs with novel and unique physicochemical properties have been extensively utilized for therapeutic applications in cancer treatment (Wiesmann et al., 2020). Different reports have shown that ZnO NPs could selectively trigger apoptosis in human cancer cells through oxidative stress (Akhtar et al., 2012; Du et al., 2023). Furthermore, Gu et al (Gu and Yang 2023) suggested that ZnO NPs are able to inhibit malignant invasion and chemotherapy resistance of cancer cells via upregulating endoplasmic reticulum stress and autophagy induction.

However, it should be emphasized that nanotoxicology as well as the development of nanostructures with specific physicochemical properties are of crucial concern with respect to the biomedical application of NPs. Several synthetic routes, including chemical, physical, and biological processes have been recommended for the synthesis of ZnO NPs (Naveed Ul Haq, 2017). Electrochemical methods have been widely used for the preparation of different inorganic NPs (Pourmortazavi et al., 2015, Yanilkin et al., 2018, Magomedova et al., 2023). Among these processes, electrodeposition is known as a feasible, affordable, and timely potential way for the synthesis of NPs (Mohanty 2011). The main advantages of the electrodeposition-mediated preparation of NPs which are the lack of complexity, low-temperature procedures, and versatility of commercial productions (Mohanty 2011). However, optimization of experimental parameters should be considered as a main issue in developing a production procedure for the synthesis of NPs.

Therefore, the novelty of this work is to fabricate ZnO NPs with a homogenous distribution and evaluate their anticancer effects against cervical cancer HeLa cells, while normal human umbilical vein endothelial cells (HUVEC) are used as a control. Also, 5-FU as a conventional anticancer drug is used as the positive control sample.

2. Materials and methods

2.1. Materials and electrochemical procedure for the synthesis of ZnO NPs

The chemical reagents were of analytical grade and purchased from the Merck Company (Darmstadt, Germany). Sodium carbonate was dissolved in deionized water to act as an electrolyte solution (0.05 M). Electrodes were polished, rinsed with alcohol, and deionized water several times. A steel electrode and zinc plate as the cathode and anode, respectively were immersed into the electrolyte solution under a direct current of 0.1 mA, voltage of 30 V, and time of 30 min at room temperature. After detaching the electrodes from the electrolyte and filtration of the solution, the obtained precipitate was exposed to washing with ethanol and deionized water several times followed by drying at 65 °C for 3 h. Finally, the samples were calcined at 700 °C for 2 h.

2.2. Characterization of ZnO NPs

X-ray diffraction (XRD) analysis was done on a Bruker, B8-advance X-ray diffractometer (voltage/current: 40 kv/30 mA) with Cu K α radiation. Scanning electron microscopy (SEM) imaging was done using a Philips XL30 series instrument. The transmission electron microscopy (TEM) imaging was performed using a JEOL JEM-2010 instrument. UV-visible (UV-vis) spectrum was read using a Jasco spectrophotometer model V-570. The particle size distribution and zeta potential of the synthesized ZnO NP solution were measured using the dynamic light scattering (DLS) technique with a Zetasizer Nano ZS 90 (Malvern Instruments Ltd., UK) instrument.

2.3. Cell lines and culture

Human cervical cancer cells (HeLa) and human umbilical vein

endothelial cells (HUVEC) were obtained from the Cell Bank of the Chinese Academy of Sciences (Shanghai, China). HeLa cells were cultured in RPMI 1640 medium (Gibco, CA, USA) containing 10 % fetal bovine serum (FBS, Gibco, CA, USA) and 1 % antibiotics at 37 °C under 5 % CO₂. HUVEC cells were cultured in a complete endothelial cell growth medium (ECGM, Provitro, Berlin, Germany) with 2 % FBS.

2.4. Cell proliferation assay

The cell viability was detected by 3-(4,5-dimethylthiazol-2-yl)-2,5-diphenyl-2H-tetrazolium bromide (MTT, Sigma-Aldrich, St. Louis, MO, USA) assay. The cells (1×10^4 cells/well) were cultured in 96-well plates and treated with different concentrations of ZnO NPs (0.01–100 $\mu\text{g/ml}$) for 24 h at 37 °C in a 5 % CO₂. Cells were then incubated with 5 mg/mL MTT solution for 4 h at 37 °C. The MTT crystal was dissolved in dimethyl sulfoxide, and cell viability was determined at 540 using a microplate reader (Thermo, MA, USA).

2.5. Quantitative real-time polymerase chain reaction (qRT-PCR) assay

qRT-PCR was utilized to assess the expression level of apoptosis-mediated mRNA. After exposure of HeLa cells with IC₅₀ concentration of ZnO NPs or standard drug 5-FU (10 μM) for 24 h, total RNA was extracted using Trizol reagent (Invitrogen, USA). Reverse transcription was done with a PrimeScript™ reverse transcriptase (Takara, Japan). Then, qRT-PCR was carried out using transcripts and a SYBR Green PCR Reagents Kit (Takara, Japan). The primer sequences were used as presented in a previous study (Huang et al., 2022). qRT-PCR amplification was done using a CFX96 real-time PCR detection system (Bio-Rad). Samples were normalized to the control GAPDH and expression folds were calculated according to equation $2^{-\Delta\Delta\text{Ct}}$.

2.6. Caspase assay

Cell apoptosis was determined using active Caspase-9 and Caspase-3 Assay Kits (Invitrogen, Carlsbad, CA, USA). Cells (2×10^5 /well) plated in a 6-well plate were treated with IC₅₀ concentration of ZnO NPs or standard drug 5-FU (10 μM) for 24 h. After that, cells were lysed in RIPA buffer, and 30 μg of total protein was utilized for the caspase-3 assay following the manufacturer's protocols.

2.7. Mitochondrial membrane potential (MMP) assay

Cells (2×10^5 cells/well) were plated in a 6-well plate and incubated with IC₅₀ concentration of ZnO NPs or standard drug 5-FU (10 μM) for 24 h. The cells were collected and then incubated with 10 μM 5,5',6,6'-tetrachloro-1,1',3,3'-tetraethylbenzimidazolcarbocyanine iodide (JC-1, Sigma-Aldrich, St. Louis, MO, USA) as a cationic fluorescent dye which exclusively localized in the mitochondria for 15 mins at room temperature in dark. Then, the cells were centrifuged for 5 mins at $500 \times g$ and pellets were washed with PBS several times and then resuspended in PBS. Finally, red (excitation 570 nm, emission 610 nm) and green (excitation 490 nm, emission 535 nm) fluorescence intensities were read on a fluorimeter (Kontron instruments SFM25, Switzerland).

2.8. Quantification of oxidative stress markers

The corresponding Assay Kits (AbCam, USA) were employed to determine different oxidative stress markers, including 3,4-Methylenedioxamphetamine (MDA, ab118970), superoxide dismutase (SOD, ab65354), catalase (CAT, ab83464), and glutathione (GSH, ab239727) in control and exposed to IC₅₀ concentrations of ZnO NPs and standard drug 5-FU (10 μM) in HeLa cells for 24 h.

2.9. ELISA analysis

After the treatment of the HeLa cells with IC₅₀ concentrations of ZnO NPs and standard drug 5-FU (10 μM) for 24 h and extraction of total protein using cell lysis assay, equal amounts of proteins were used for determination of cytochrome c release using an ELISA Kit (AbCam, USA) according to the manufacturer's protocol.

2.10. Statistical analysis

All assays for the cellular part were done in triplicate, and data were reported as mean ± SD. All data analyses were carried out using SPSS software and the statistical significance was performed with one-way ANOVA followed by Tukey's test. $P < 0.05$ was considered statistically significant.

3. Result and discussion

The electrochemical approach has been widely used for the preparation of ZnO NPs of various sizes and shapes (Anand and Srivastava 2015, Pourmortazavi et al., 2015, Jose et al., 2018). Several parameters such as pH, concentration of electrolyte, voltage, and conductivity can play a key role in the physicochemical properties of synthesized ZnO NPs through electrochemical method (Anand and Srivastava 2015).

Fig. 1 displays the XRD pattern of ZnO NPs prepared by the electrodeposition method. XRD peaks were observed to be sharp and well-defined, designating good crystallinity and homogeneity of the prepared NPs. Additionally, the lack of secondary peaks clarifies the good purity of the synthesized ZnO NPs.

The diffraction peaks presented at 31.65, 35.00, 36.85, 47.95, 56.55, 63.95, 66.55, 67.70, 69.10, 73.65, and 77.45° are indexed to lattice planes (h, l, k) of (1 0 0), (0 0 2), (1 0 1), (1 0 2), (1 1 0), (1 0 3), (2 0 0), (1 1 2), (2 0 1), (0 0 4), and (2 0 2), respectively, which are indicative of a hexagonal wurtzite phase of ZnO NPs (Imade et al., 2022).

The formation of ZnO NPs was also confirmed by standard JCPDS Card no. JCPDS-36-1451 (Singh, Singh et al. 2023). The XRD data are aligned with the results reported previously for the synthesis of ZnO NPs through the electrodeposition method (Giri et al. 2023) and verify the production of highly pure ZnO NPs.

The surface morphology of the electrodeposited synthesized ZnO NPs was analyzed using an SEM instrument. Fig. 2a displays the SEM image of ZnO NPs which unveiled homogeneous spherical/hexagonal-like structures of the prepared NPs. In general, the micrograph demonstrated that the system has NPs in a well-defined pattern, suggesting that the distinct homogenous samples have been produced through the electrodeposition method (Anand and Srivastava 2015).

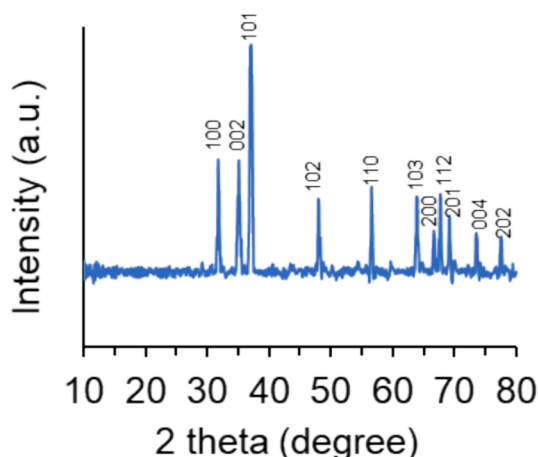


Fig. 1. The XRD pattern of ZnO NPs prepared by the electrodeposition method.

Fig. 2b displays the TEM image of the synthesized ZnO NPs produced by the electrodeposition method. ZnO NPs with an average diameter of about 8 nm were observed by an image taken by a TEM apparatus. The morphology of the ZnO NPs could be studied by TEM, and it was found that they had a nearly spherical or hexagonal shape. The TEM image of ZnO NPs obtained from the electrolyte concentration of 30 mM or 60 mM NaHCO₃ at 1 A/dm² along with calcination at 600 °C for 1 h showed that particles possessed a clear spindle-like morphology with an average NP size ranging from 30-40 nm (Chandruppa and Venkatesha 2012). These differences between the previous reported TEM and our result can be due to different calcination times, concentrations of bicarbonate, and experimental setup.

The optical properties and electronic band gap energy of (E_g) of synthesized ZnO NPs were assessed using UV-Vis spectroscopy. The UV-Vis absorption spectroscopy is known as a simple and sensitive strategy to investigate the synthesis of NPs. The UV-Vis absorption spectrum of the electrodeposited synthesized ZnO NPs is represented in Fig. 3. The absorption spectrum shows a characteristic absorption band of ZnO NPs around the maximum wavelength of 368 nm (3), confirming the successful synthesis of ZnO NPs (Geetha et al., 2016).

The band gap energy (E_g) of synthesized ZnO NPs for electronic transitions was determined by using the following Equation (1):

$$E_g = 1240/\lambda_{\max} \quad (1)$$

where λ_{\max} is the maximum adsorption wavelength (368 nm). Therefore, the E_g value was determined to be around 3.36 eV, which is almost in good agreement with previous studies reporting the synthesis of ZnO NPs by the sol-gel (Manikandan et al., 2018) or solution combustion methods (Nagaraju et al., 2017).

The particle size of synthesized ZnO NPs in solution was determined by the DLS instrument, which is able to measure the particle size of NPs dissolved in liquids (Yedurkar, Maurya et al. 2016). The average size along with the size distribution of the electrodeposited synthesized ZnO were measured by DLS and the result is shown in Fig. 4a. The obtained particle size of ZnO NPs shows the diameter distribution starting from 18 to 43 nm. It reveals the average NP size of 29.24 nm which is not in good agreement with the TEM (8 nm) analysis outcome. This discrepancy comes from obtaining the average size of NPs in the powder and dispersed forms by TEM and DLS, respectively.

Additionally, zeta potential analysis was performed to determine the surface charges attained by ZnO NPs, which can find a use for further understanding of the stability of the colloidal samples. The magnitude of the zeta potential value is known as a basis of the potential stability of NP colloid suspension (Yedurkar et al. 2016). If the NPs in a suspended form show high zeta potential values (both negative and positive), NPs will tend to repel each other and no agglomeration occurs (Yedurkar et al. 2016). However, there is no force to inhibit particles from aggregating if their zeta potential values are low. It is typically accepted that if the zeta potential values are greater/smaller than +30 mV/−30 mV, the obtained suspensions will be stable (Huo et al. 2019, Carone et al. 2023). The zeta potential value of the electrodeposited synthesized ZnO NPs was determined to have a distribution starting from +5 to −43 mV with an average zeta potential value of −19 mV as shown in Fig. 4b. This data indicates that there are moderate repulsion forces between the NPs, which moderately improve the stability of the ZnO NPs.

In general, the formation mechanism of NPs via electrodeposition is explained by Golsheikh et al. (Golsheikh et al. 2013). The positively-charged Zn ions can be adsorbed on the negatively-charged electrode and reduced to ZnO NPs by using a negative potential. Also, the Zn ions in the aqueous solution can be deposited and reduced on the formed ZnO NPs, which could cause the growth of the initially produced ZnO NPs or nucleation of new ZnO NPs (Golsheikh, Huang et al. 2013).

3.1. Cell viability assay

Cancer cells with an outstanding extent of self-replication and

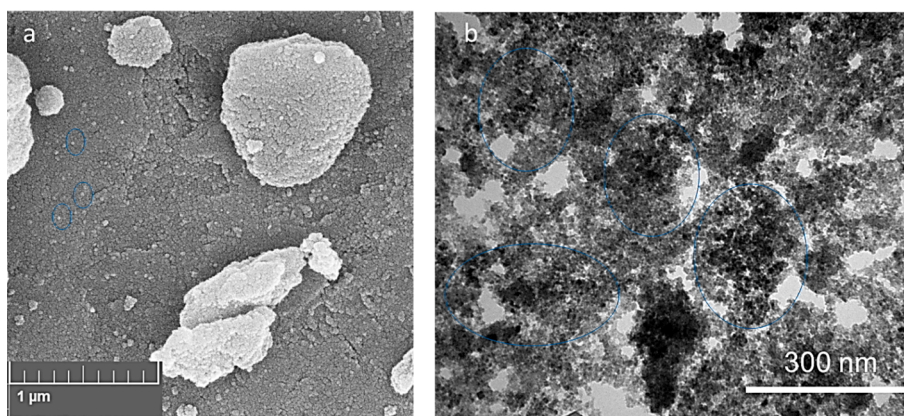


Fig. 2. The SEM (a) and TEM (b) images of ZnO NPs prepared by the electrodeposition method.

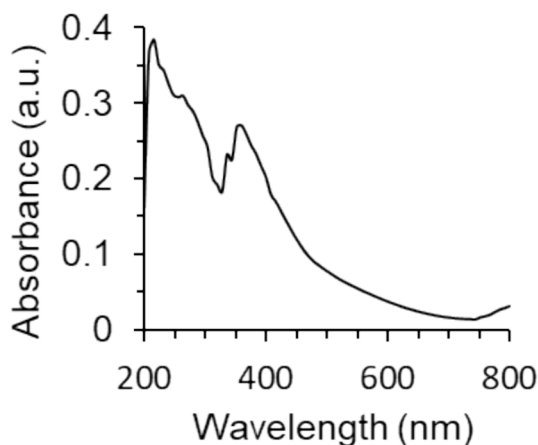


Fig. 3. The UV-visible spectrum of ZnO NPs prepared by the electrodeposition method.

uncontrolled cell proliferation result in the formation of invasion tissues (Krakhmal et al. 2015). The potency and safety of cancer treatment by anticancer drugs have faced a main challenge, low selectivity, which induces cytotoxicity in both cancerous and non-malignant cells (Fouad and Aanei 2017). To address these concerns and boost the potency of cancer treatment, NP-based platforms have been developed (Verma et al. 2023). In this study, to assess the anticancer characteristics of the electrodeposited synthesized ZnO NPs, we utilized the well-known MTT assay to detect if these NPs are able to inhibit selectively the growth of human cervical cancer HeLa cells versus human umbilical vein endothelial cells, HUVEC. Our results indicated that the growth of HeLa cells was significantly decreased upon incubation with ZnO NPs at different

concentrations of 10, 50 and 100 $\mu\text{g}/\text{mL}$, however, these concentrations did not trigger significant cytotoxic effect on HUVEC non-malignant cells (Fig. 5). These data showed that ZnO NPs are selectively cytotoxic to cervical cancer HeLa cells (Fig. 5). Given that 35.40 $\mu\text{g}/\text{mL}$ of ZnO NPs could inhibit 50 % of the HeLa cell viability, this concentration was used for the further ongoing assays.

Chen et al. (Chen et al. 2021) showed that ZnO NPs synthesized from *Aspergillus terreus* had a mean size of 43.72 nm with an IC_{50} concentration of 20.43 $\mu\text{g}/\text{mL}$ against HeLa cells. However, they found that ZnO NPs at 70 $\mu\text{g}/\text{mL}$ exhibited remarkable cytotoxicity on normal cells (Chen, Luo et al. 2021). Also, Wahab et al. (Wahab et al., 2011) reported that synthesized ZnO NPs with a size in the range of 20 to 30 nm had an IC_{50} value of about 118 $\mu\text{g}/\text{mL}$ against HeLa cells after 24 h. Additionally, Thomas et al. (Thomas et al. 2022) revealed that biosynthesized ZnO NPs with an average particle size ranging from 30.8 to 86.8 nm had a significant anticancer activity against HeLa cells with an IC_{50} value of 31.6 $\mu\text{g}/\text{mL}$.

3.2. Apoptosis analysis

In order to study whether the anti-proliferation activity of ZnO NPs in HeLa cells was triggered by cell apoptosis, qRT-PCR and caspase activity assays as gold standards for cell apoptosis investigation, were conducted.

The apoptosis-triggering Bcl-2 family promotes mitochondrial-mediated apoptosis (Martinou and Youle 2011, Czabotar and Garcia-Saez 2023). Bax and Bcl-2 play a key role in the induction of apoptosis, as Bax expression on the mitochondrial membrane increases and the Bcl-2 expression reduces (Czabotar and Garcia-Saez 2023). Caspase-9 is responsible for the formation of apoptotic bodies which are mediators of caspase-3 activation known as a typically distributed enzyme in the process of apoptosis (Brentnall et al. 2013). In this study,

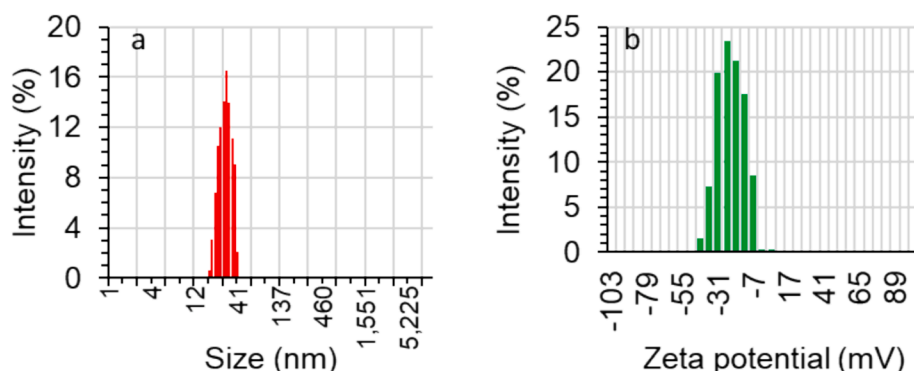


Fig. 4. The DLS (a) and zeta potential (b) of ZnO NPs prepared by the electrodeposition method.

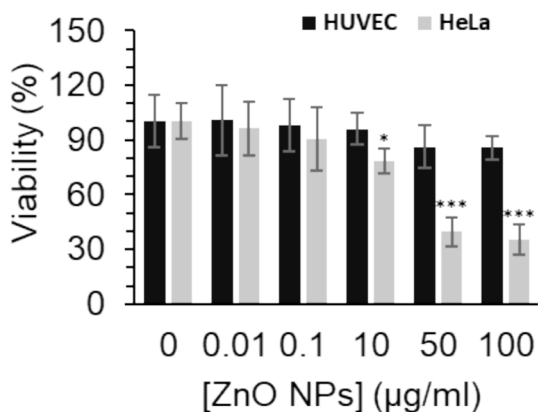


Fig. 5. The effect of different concentrations of synthesized ZnO NPs prepared by the electrodeposition method on the proliferation of human cervical cancer HeLa cells versus human umbilical vein endothelial cells, HUVEC, after 24 h. The data are expressed as mean \pm SD of three experiments. * $P < 0.05$, *** $P < 0.001$ relative to control.

we tried to assess the molecular expression levels of four genes (Bax, Bcl-2, caspase-9, and caspase-3) by qRT-PCR assay to confirm whether ZnO NPs could influence the expression levels of apoptosis-mediated mRNA. As shown in Fig. 6, the qRT-PCR findings revealed that ZnO NPs decreased the expression level of Bcl2 mRNA (Fig. 6a), while the gene expression levels of Bax (Fig. 6b), caspase-9 (Fig. 6c), and caspase-3 (Fig. 6d) in HeLa cells were upregulated. Chen et al. (Chen, Luo et al. 2021) also indicated that following incubation of HeLa cells with ZnO NPs synthesized from *Aspergillus terreus* Bcl-2 expression remarkably decreased, whereas, the expression levels of Bax, caspase-9, and caspase-3 were notably upregulated. Yang et al. also demonstrated that the synthesized ZnO quantum dot NPs with a diameter of around 7 nm stimulated apoptosis in HeLa cells through considerable changes in the expression levels of Bax, Bcl-2, caspase-9, and caspase-3 genes (Yang et al., 2020).

Moreover, the effects of ZnO NPs on caspase-9 and caspase-3 activity in HeLa cells were explored. In comparison to untreated cells, HeLa cells incubated with IC₅₀ concentration of ZnO NPs (35.40 µg/mL) demonstrated a significant increase in caspase-9 (Fig. 6e) and caspase-3 activities (Fig. 6f), which were also observed in the 5-FU-treated HeLa cells. As a result, it was found that ZnO NP incubation triggered

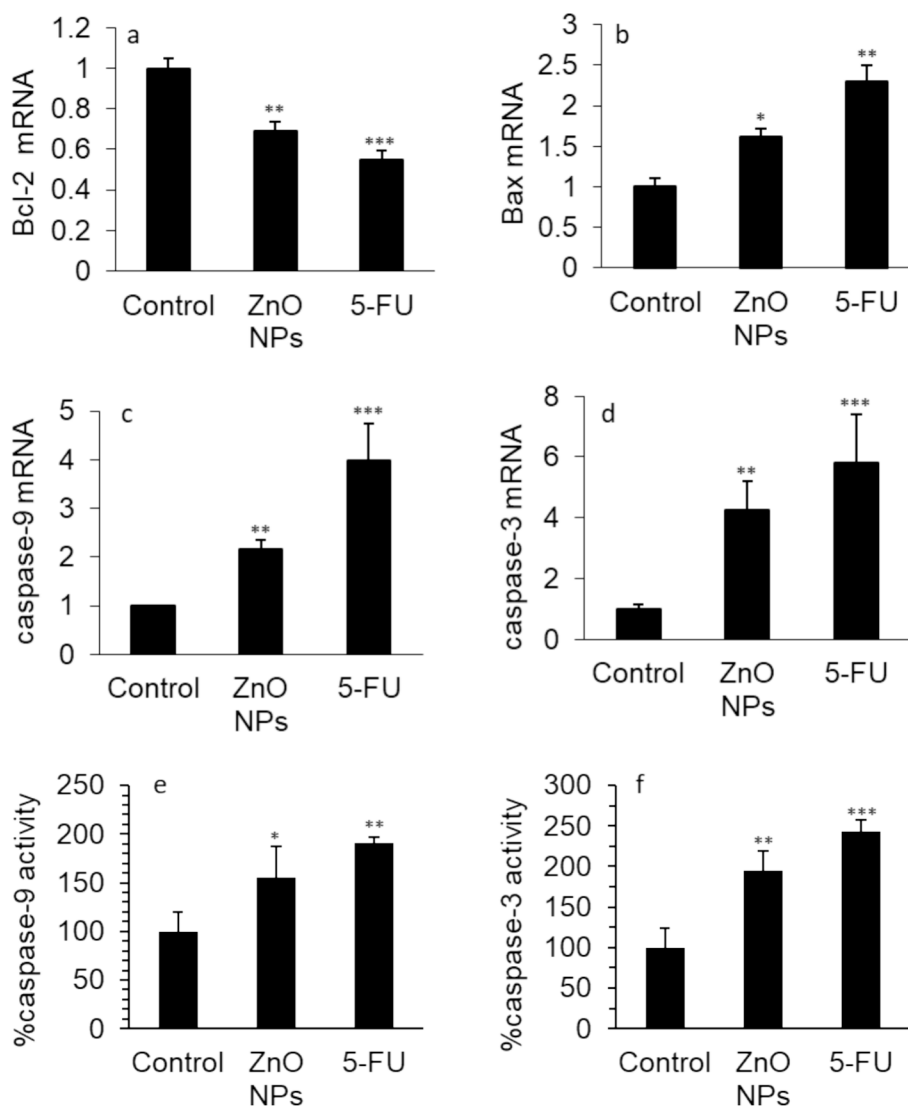


Fig. 6. The effect of 35.40 µg/mL synthesized ZnO NPs prepared by the electrodeposition method or standard drug 5-FU (10 µM) on the (a) Bcl-2 mRNA expression, (b) Bax mRNA expression, (c) caspase-9 mRNA expression, (d) caspase-3 mRNA expression, (e) caspase-9 activity, (f) caspase-3 activity in human cervical cancer HeLa cells after 24 h. The data are expressed as mean \pm SD of three experiments. * $P < 0.05$, ** $P < 0.01$, *** $P < 0.001$ relative to control.

apoptosis induction in the HeLa cells.

Hence, the results of the caspase-9 (Fig. 6e) and caspase-3 (Fig. 6f) activity assays were consistent with the qRT-PCR outcomes and also findings reported by Chen et al. (Chen, Luo et al. 2021), which revealed that caspase-9 and caspase-3 activities were enhanced following interaction of synthesized NPs with HeLa cells.

Therefore, the finding showed that the levels of apoptosis markers were altered in ZnO NPs- or 5-FU-treated HeLa cells in comparison to control cells.

3.3. Oxidative stress evaluation

The exposure to ZnO NPs could induce cytotoxicity in human carcinoma cells through oxidative stress-mediated apoptosis (De Berardis et al. 2010, Wahab et al. 2013, Shochah and Jabir 2023). For example, Khan et al. (Khan et al., 2021) proposed that ZnO NPs trigger apoptosis in epidermoid carcinoma cells mediated by oxidative stress and DNA degradation. Shochah et al. also reported that biosynthesized gold/ZnO NPs can induce anticancer effects against breast cancer MCF-7 cells through oxidative stress (Shochah and Jabir 2023). Therefore, we aimed to evaluate the production of MDA products as a typical marker of oxidative stress and the levels of SOD activity, CAT activity, and GSH contents as main markers of antioxidant molecules (Rayzah et al. 2023).

The effects of ZnO NP and 5-FU incubation on the MDA production, SOD activity, CAT activity, and GSH content in HeLa cells are depicted in Fig. 7. The level of MDA notably increased in HeLa cells, which were exposed to IC₅₀ concentration of ZnO NPs (35.40 µg/mL) for 24 h (Fig. 7a).

Furthermore, the SOD activity (Fig. 7b), CAT activity (Fig. 7c), and GSH level (Fig. 7d) were markedly reduced by the IC₅₀ concentration of ZnO NPs. The treatment of the HeLa cells with 5-FU also elevated the production of MDA level while mitigating the SOD activity, CAT activity, and GSH level in the HeLa cells (Fig. 7). These findings proved that ZnO NPs treatment decreases antioxidant systems while elevating the MDA level, thereby facilitating oxidative stress-regulated cell death in cancer cells.

Based on the literature survey, lipid peroxidation (formation of

MDA) has been shown to be a main consequence of oxidative stress, which is promoted by the excessive presence of free radicals (Farmer and Mueller 2013). The increased level of lipid peroxidation induced by oxidative stress and reduced amounts of endogenous antioxidant molecules could lead to apoptosis/autophagy/ferroptosis induction in cancer cells (Farmer and Mueller 2013). In this study, we found that the elevated MDA formation and diminished activities/contents of antioxidant molecules in HeLa cells could occur following incubation of cells with electrodeposited synthesized ZnO NPs. Oxidative stress-mediated ZnO NPs could derive from the unnecessary formation of dissolved zinc ions, giving rise to the elevated intracellular oxidative stress in cancer cells followed by the initiation of apoptosis via different apoptotic signaling pathways (Chen et al. 2021). In fact, released ions can serve as pro-oxidants mediated by Fenton and Fenton-like reactions to promote the excessive generation of hydroxyl free radicals (Han et al. 2023). The Bax, Bcl-2, caspase-9, and caspase-3 expression can be changed by the oxidative stress markers, which may cause macromolecular damage in cancer cells and induction of apoptosis (Sanati et al. 2022).

3.4. Mitochondrial apoptotic pathway

MMP modulates matrix arrangement and cytochrome c release upon the intrinsic apoptosis pathway (Gottlieb et al. 2003). Cytochrome c has multiple functions ranging from its role in life regulation and death programs of the cells (Hüttemann et al. 2011). Therefore, inhibition of the mitochondrial-mediated apoptosis occurs through blocking MMP loss and cytochrome c release (Koya et al. 2000).

To explore the underlying mitochondrial-mediated mechanism contributes to ZnO NPs-stimulated apoptosis in cervical cancer HeLa cells, JC-1 staining was done to assess the MMP reduction. In Fig. 8a, in comparison with the control group, the MMP significantly decreased upon the interaction of cells with ZnO NPs at 24 h, which was representative of an event in the early stage of cell apoptosis mediated by mitochondrial damage (Hu et al. 2021). The finding was also consistent with the detection of apoptosis revealed by qTR-PCR and caspase assays.

It is well known that the mitochondrial-mediated apoptosis pathway

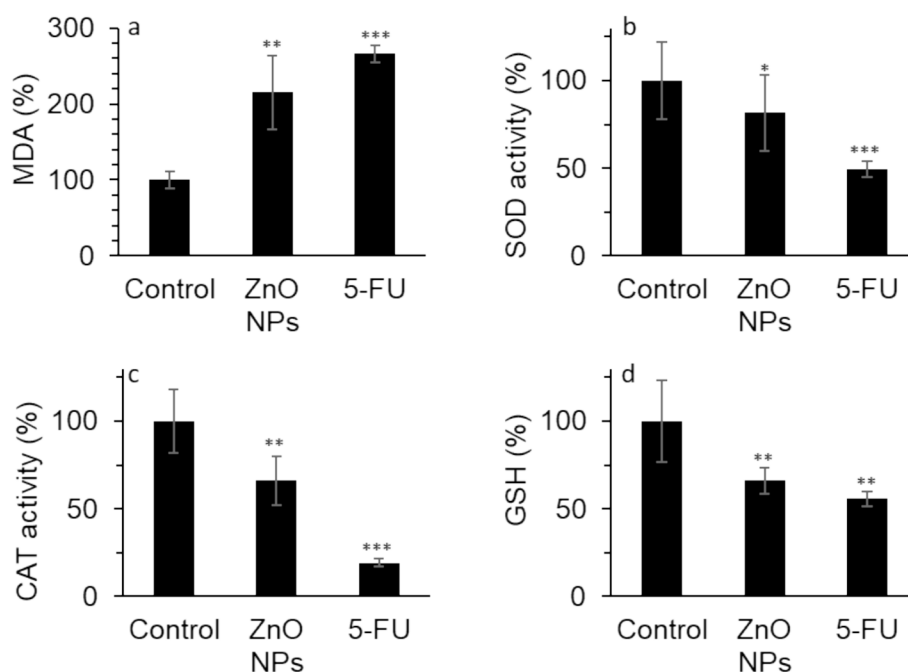


Fig. 7. The effect of 35.40 µg/mL synthesized ZnO NPs prepared by the electrodeposition method or standard drug 5-FU (10 µM) on the (a) MDA level, (b) SOD activity, (c) CAT activity, (d) GSH content in human cervical cancer HeLa cells after 24 h. The data are expressed as mean ± SD of three experiments. *P<0.05, **P<0.01, ***P<0.001 relative to control.

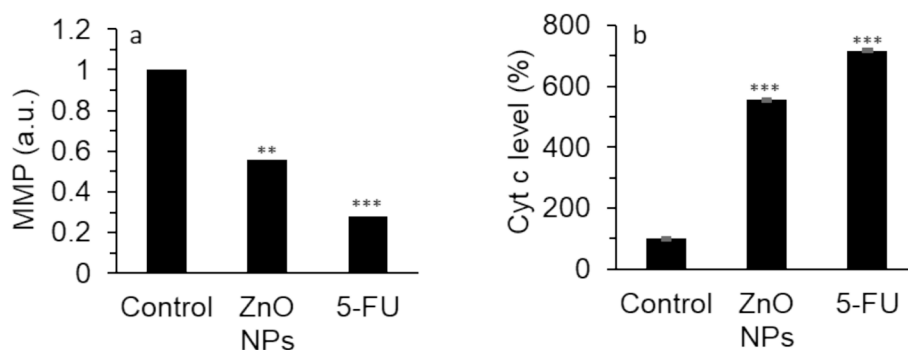


Fig. 8. The effect of 35.40 $\mu\text{g/mL}$ synthesized ZnO NPs prepared by the electrodeposition method or standard drug 5-FU (10 μM) on the (a) MMP level, (b) cytochrome *c* protein level in human cervical cancer HeLa cell cytoplasm after 24 h. The data are expressed as mean \pm SD of three experiments. ** $P < 0.01$, *** $P < 0.001$ relative to control.

plays a crucial role in the apoptosis, and cytochrome *c* serves as an Achilles' heel in this process (Kulikova et al. 2012).

Then, the level of cytoplasmic cytochrome *c* was determined by ELISA assay, which is a vital biomarker in the induction of mitochondrial-mediated apoptosis. In Fig. 8b, the level of cytochrome *c* in cytoplasm was increased upon the interaction of HeLa cells with ZnO NPs which was comparable to the effect of 5-FU. In fact, in the mitochondrial-mediated apoptotic pathway, altered expression of Bax and Bcl-2 markers could result in cytochrome *c* release from mitochondria to cytoplasm to activate caspase-9/caspase-3 signaling cascade (Scorrano and Korsmeyer 2003, Tutuncu and Ozdemir 2023).

In general, following the incubation of HeLa cells with ZnO NPs at 24 h, the expression levels of Bcl-2 and Bax mRNA were altered, and caspase-9 and caspase-3 mRNA expression and associated activities were enhanced. Further investigations showed that MMP loss and cytochrome *c* release were triggered after incubation of HeLa cells with ZnO NPs. According to the above data, we might conclude that the mitochondrial-mediated apoptosis signaling pathway contributes to the ZnO NPs-induced apoptosis mechanism in HeLa cells.

4. Conclusion

In conclusion, ZnO NPs synthesized via the electrodeposition method showed homogeneous spherical/hexagonal-like structures with an average diameter of about 8 nm. Also, ZnO NPs caused a significant anticancer activity against cervical cancer HeLa cells through induction of oxidative stress and changes of main apoptotic markers in the mitochondrial-mediated apoptosis signaling pathway. In conclusion, these data may hold great promise for the integration of electrodeposited synthesized ZnO NPs with other chemotherapeutics in cervical cancer HeLa cells to develop potential anticancer agents, which needs further *in vitro* and *in vivo* studies in future plans. It should be noted that the main part of this research was conducted on HeLa cells, which may not be a representative sample of all types of cervical cancer. As a result, the data may not generalize to other cancer cell lines or types, requiring additional research using a wider range of cell models. Future research should also be done to explore the long-term effects of ZnO NP treatment, such as potential resistance development or chronic toxicity, which are crucial for assessing the feasibility of therapeutic applications. Furthermore, it is important to assess the environmental effects and biocompatibility of ZnO NPs with different physicochemical properties in order to ensure their broad application.

Funding

This study was supported by Zhejiang Natural Science Foundation Public Welfare Project (ID: LGH20H160022), and the Enze Major Project Fund.

CRediT authorship contribution statement

Yingying Chen: Methodology, Investigation, Data curation. **Xinxin You:** Methodology, Investigation, Data curation. **Liya Ye:** Writing – original draft, Conceptualization. **Shuangshuang Mei:** Project administration, Conceptualization, Methodology. **Junhui Yu:** Resources, Formal analysis, Conceptualization. **Youyou Xie:** Writing – review & editing, Conceptualization. **Kai Wang:** Writing – review & editing, Conceptualization. **Xing Chen:** Writing – review & editing, Validation, Supervision, Resources, Conceptualization.

Declaration of Competing Interest

The authors declare that they have no known competing financial interests or personal relationships that could have appeared to influence the work reported in this paper.

Acknowledgements

Not applicable.

References

- Akhtar, M. J., M. Ahamed, S. Kumar, M. A. M. Khan, J. Ahmad and S. A. Alrokayan (2012). "Zinc oxide nanoparticles selectively induce apoptosis in human cancer cells through reactive oxygen species." *International journal of nanomedicine*: 845-857.
- Anand, V., Srivastava, V.C., 2015. Zinc oxide nanoparticles synthesis by electrochemical method: Optimization of parameters for maximization of productivity and characterization. *J. Alloy. Compd.* 636, 288-292.
- Brentnall, M., Rodriguez-Menocal, L., De Guevara, R.L., Cepero, E., Boise, L.H., 2013. Caspase-9, caspase-3 and caspase-7 have distinct roles during intrinsic apoptosis. *BMC Cell Biol.* 14, 1-9.
- Burmeister, C.A., Khan, S.F., Schäfer, G., Mbatani, N., Adams, T., Moodley, J., Prince, S., 2022. Cervical cancer therapies: Current challenges and future perspectives. *Tumour Virus Research* 13, 200238.
- Carone, A., Emilsson, S., Mariani, P., Désert, A., Parola, S., 2023. Gold nanoparticle shape dependence of colloidal stability domains. *Nanoscale Advances* 5 (7), 2017-2026.
- Chandrapa, K.G., Venkatesha, T.V., 2012. Electrochemical synthesis and photocatalytic property of zinc oxide nanoparticles. *Nano-Micro Letters* 4, 14-24.
- Chen, H., Luo, L., Fan, S., Xiong, Y., Ling, Y., Peng, S., 2021. Zinc oxide nanoparticles synthesized from *Aspergillus terreus* induces oxidative stress-mediated apoptosis through modulating apoptotic proteins in human cervical cancer HeLa cells. *J. Pharm. Pharmacol.* 73 (2), 221-232.
- Cohen, P.A., Jhingran, A., Oaknin, A., Denny, L., 2019. Cervical cancer. *Lancet* 393 (10167), 169-182.
- Czabotar, P.E., Garcia-Saez, A.J., 2023. Mechanisms of BCL-2 family proteins in mitochondrial apoptosis. *Nat. Rev. Mol. Cell Biol.* 24 (10), 732-748.
- De Berardis, B., Civitelli, G., Condello, M., Lista, P., Pozzi, R., Arancia, G., Meschini, S., 2010. Exposure to ZnO nanoparticles induces oxidative stress and cytotoxicity in human colon carcinoma cells. *Toxicol. Appl. Pharmacol.* 246 (3), 116-127.
- Du, W., Feng, K., Li, C., Li, S., Abidin, Z.U., Yin, H., Chen, S., 2023. Controlled synthesis of zinc oxide nanoparticles through flame spray pyrolysis and evaluation of their anticancer effects against gastric cancer cell. *Arab. J. Chem.* 16 (10), 105192.
- Farmer, E.E., Mueller, M.J., 2013. ROS-mediated lipid peroxidation and RES-activated signaling. *Annu. Rev. Plant Biol.* 64, 429-450.
- Fouad, Y.A., Aanei, C., 2017. Revisiting the hallmarks of cancer. *Am. J. Cancer Res.* 7 (5), 1016.

- Geetha, M., Nagabhushana, H., Shivananjai, H., 2016. Green mediated synthesis and characterization of ZnO nanoparticles using Euphorbia Jatropa latex as reducing agent. *J. Sci.: Adv. Mater. Devices* 1 (3), 301–310.
- Giri, P.M., Banerjee, A., Layek, B., 2023. A Recent Review on Cancer Nanomedicine. *Cancers* 15 (8), 2256.
- Golsheikh, A.M., Huang, N., Lim, H., Zakaria, R., Yin, C.-Y., 2013. One-step electrodeposition synthesis of silver-nanoparticle-decorated graphene on indium-tin-oxide for enzymeless hydrogen peroxide detection. *Carbon* 62, 405–412.
- Gottlieb, E., Armour, S., Harris, M., Thompson, C., 2003. Mitochondrial membrane potential regulates matrix configuration and cytochrome c release during apoptosis. *Cell Death Differ.* 10 (6), 709–717.
- Gu, W., Yang, C., 2023. Zinc oxide nanoparticles inhibit malignant progression and chemotherapy resistance of ovarian cancer cells by activating endoplasmic reticulum stress and promoting autophagy. *Exp. Ther. Med.* 26 (5), 1–11.
- Han, H., Li, J., Santos, H.A., 2023. Recent advances in Fenton and Fenton-like reaction mediated nanoparticle in cancer therapy. *Biomedical Technology* 3, 40–51.
- Naveed Ul Haq, A., A. Nadhman, I. Ullah, G. Mustafa, M. Yasinzai and I. Khan (2017). "Synthesis approaches of zinc oxide nanoparticles: the dilemma of ecotoxicity." *Journal of Nanomaterials* 2017.
- Hu, Z., Wang, H., Fu, Y., Ma, K., Ma, X., Wang, J., 2021. Gentiopicroside inhibits cell growth and migration on cervical cancer via the reciprocal MAPK/Akt signaling pathway. *Nutr. Cancer* 73 (8), 1459–1470.
- Huang, X., Yan, P., Ding, W., Zhou, C., Xu, Q., Li, M., Ye, L., Chen, W., 2022. α -Pinene inhibits the growth of cervical cancer cells through its proapoptotic activity by regulating the miR-34a-5p/Bcl-2 signaling axis. *Drug Dev. Res.* 83 (8), 1766–1776.
- Huo, W., Zhang, X., Gan, K., Chen, Y., Xu, J., Yang, J., 2019. Effect of zeta potential on properties of foamed colloidal suspension. *J. Eur. Ceram. Soc.* 39 (2–3), 574–583.
- Hüttemann, M., Pecina, P., Rainbolt, M., Sanderson, T.H., Kagan, V.E., Samavati, L., Doan, J.W., Lee, I., 2011. The multiple functions of cytochrome c and their regulation in life and death decisions of the mammalian cell: From respiration to apoptosis. *Mitochondrion* 11 (3), 369–381.
- Imade, E.E., Ajiboye, T.O., Fadiji, A.E., Onwudiwe, D.C., Babalola, O.O., 2022. Green synthesis of zinc oxide nanoparticles using plantain peel extracts and the evaluation of their antibacterial activity. *Scientific African* 16, e01152.
- Jose, A., Devi, K.R.S., Pinheiro, D., Narayana, S.L., 2018. Electrochemical synthesis, photodegradation and antibacterial properties of PEG capped zinc oxide nanoparticles. *J. Photochem. Photobiol. B Biol.* 187, 25–34.
- Khan, M.J., Ahmad, A., Khan, M.A., Siddiqui, S., 2021. Zinc oxide nanoparticle induces apoptosis in human epidermoid carcinoma cells through reactive oxygen species and DNA degradation. *Biol. Trace Elem. Res.* 199, 2172–2181.
- Kissel, M., Rambeau, A., Achkar, S., Lecuru, F., Mathevet, P., 2020. Challenges and advances in cervix cancer treatment in elder women. *Cancer Treat. Rev.* 84, 101976.
- Koya, R.C., Fujita, H., Shimizu, S., Ohtsu, M., Takimoto, M., Tsujimoto, Y., Kuzumaki, N., 2000. Gelsolin inhibits apoptosis by blocking mitochondrial membrane potential loss and cytochrome c release. *J. Biol. Chem.* 275 (20), 15343–15349.
- Krakhmal, N.V., Zavyalova, M.V., Denisov, E.V., Vtorushin, S.V., Perelmutter, V.M., 2015. Cancer invasion: patterns and mechanisms. *Acta Naturae (англоязычная Версия)* 7 (2 (25)), 17–28.
- Kulikov, A., Shilov, E., Mufazalov, I., Gogvadze, V., Nedospasov, S., Zhivotovsky, B., 2012. Cytochrome c: the Achilles' heel in apoptosis. *Cell. Mol. Life Sci.* 69, 1787–1797.
- Magomedova, A., Isaev, A., Orudzhiev, F., Alikhanov, N., Emirov, R., Rabadanov, M., Mingshan, Z., 2023. Electrochemical Synthesis of Superparamagnetic Fe₃O₄ Nanoparticles for the Photo-Fenton oxidation of Rhodamine B. *ChemistrySelect* 8 (30), e202301694.
- Manikandan, B., Endo, T., Kaneko, S., Murali, K.R., John, R., 2018. Properties of sol gel synthesized ZnO nanoparticles. *J. Mater. Sci. Mater. Electron.* 29, 9474–9485.
- Martinou, J.-C., Youle, R.J., 2011. Mitochondria in apoptosis: Bcl-2 family members and mitochondrial dynamics. *Dev. Cell* 21 (1), 92–101.
- Mohanty, U.S., 2011. Electrodeposition: a versatile and inexpensive tool for the synthesis of nanoparticles, nanorods, nanowires, and nanoclusters of metals. *J. Appl. Electrochem.* 41, 257–270.
- Movva, S., Rodriguez, L., Arias-Pulido, H., Verschraegen, C., 2009. "Novel chemotherapy approaches for cervical cancer." *Cancer: Interdisciplinary International Journal of the Am. Cancer Soc.* 115 (14), 3166–3180.
- Nagaraju, G., Shivaraju, G., Banuprakash, G., Rangappa, D., 2017. Photocatalytic activity of ZnO nanoparticles: synthesis via solution combustion method. *Mater. Today: Proc.* 4 (11), 11700–11705.
- Naser, S.S., Ghosh, B., Simnani, F.Z., Singh, D., Choudhury, A., Nandi, A., Sinha, A., Jha, E., Panda, P.K., Suar, M., 2023. Emerging trends in the application of green synthesized biocompatible ZnO nanoparticles for translational paradigm in cancer therapy. *Journal of Nanotheranostics* 4 (3), 248–279.
- Pourmortazavi, S.M., Marashianpour, Z., Karimi, M.S., Mohammad-Zadeh, M., 2015. Electrochemical synthesis and characterization of zinc carbonate and zinc oxide nanoparticles. *J. Mol. Struct.* 1099, 232–238.
- Pugazhendhi, A., Edison, T.N.J.L., Karuppusamy, I., Kathirvel, B., 2018. Inorganic nanoparticles: a potential cancer therapy for human welfare. *Int. J. Pharm.* 539 (1–2), 104–111.
- Rayzah, M., Elderderly, A.Y., Alzerwi, N.A.N., Alzahrani, B., Alsrhani, A., Alsultan, A., Idrees, B., Rayzah, F., Bakhsh, Y., Alzahrani, A.M., 2023. Syzygium cumini (L.) Extract-Derived Green Titanium Dioxide Nanoparticles Induce Caspase-Dependent Apoptosis in Hepatic Cancer Cells. *Plants* 12 (18), 3174.
- Sanati, M., Afshari, A.R., Kesharwani, P., Sukhorukov, V.N., Sahebkar, A., 2022. Recent trends in the application of nanoparticles in cancer therapy: The involvement of oxidative stress. *J. Control. Release* 348, 287–304.
- Scorrano, L., Korsmeyer, S.J., 2003. Mechanisms of cytochrome c release by proapoptotic BCL-2 family members. *Biochem. Biophys. Res. Commun.* 304 (3), 437–444.
- Shanmugam, S., Susikar, S., Pravenkumar, R.R., 2023. Neoadjuvant Chemotherapy Followed by Surgery in FIGO Stage IB2, IIA2, and IIB Cervical Cancer—Survival Analysis. *Indian Journal of Gynecologic Oncology* 21 (3), 56.
- Shochah, Q.R., Jabir, F.A., 2023. Green synthesis of Au/ZnO nanoparticles for anticancer activity and oxidative stress against MCF-7 cell lines. *Biomass Convers. Biorefin.* 1–14.
- Singh, N., Singh, R., Shah, K., Pramanik, B.K., 2023. Green synthesis of zinc oxide nanoparticles using lychee peel and its application in anti-bacterial properties and CR dye removal from wastewater. *Chemosphere* 327, 138497.
- Thomas, S., Gunasankaran, G., Arumugam, V.A., Muthukrishnan, S., 2022. Synthesis and characterization of zinc oxide nanoparticles of solanum nigrum and its anticancer activity via the induction of apoptosis in cervical cancer. *Biol. Trace Elem. Res.* 200 (6), 2684–2697.
- Tutuncu, S., Ozdemir, B., 2023. Fundamental Molecules in the Pathways and Regulation of Apoptosis. *International Journal of Veterinary and Animal Research (IJVAR)* 6 (1), 35–38.
- Varlotto, J.M., Cardarelli, G.A., 2023. Recent advances in cervical cancer radiotherapy. *Front. Oncol.* 13, 1144797.
- Verma, J., Warsame, C., Seenivasagam, R.K., Katiyar, N.K., Aleem, E., Goel, S., 2023. Nanoparticle-mediated cancer cell therapy: Basic science to clinical applications. *Cancer Metastasis Rev.* 1–27.
- Wahab, R., Kaushik, N.K., Verma, A.K., Mishra, A., Hwang, I.H., Yang, Y.-B., Shin, H.-S., Kim, Y.-S., 2011. Fabrication and growth mechanism of ZnO nanostructures and their cytotoxic effect on human brain tumor U87, cervical cancer HeLa, and normal HEK cells. *J. Biol. Inorg. Chem.* 16, 431–442.
- Wahab, R., Dwivedi, S., Umar, A., Singh, S., Hwang, I.H., Shin, H.-S., Musarrat, J., Al-Khedhairi, A.A., Kim, Y.-S., 2013. ZnO nanoparticles induce oxidative stress in Cloudman S91 melanoma cancer cells. *J. Biomed. Nanotechnol.* 9 (3), 441–449.
- Wiesmann, N., Tremel, W., Brieger, J., 2020. Zinc oxide nanoparticles for therapeutic purposes in cancer medicine. *J. Mater. Chem. B* 8 (23), 4973–4989.
- Wolfram, J., Ferrari, M., 2019. Clinical cancer nanomedicine. *Nano Today* 25, 85–98.
- Yang, Y., Song, Z., Wu, W., Xu, A., Lv, S., Ji, S., 2020. ZnO quantum dots induced oxidative stress and apoptosis in HeLa and HEK-293T cell lines. *Front. Pharmacol.* 11, 131.
- Yanilkina, V.V., Gul'naz, R.N., Kokorekin, V.A., 2018. Mediated electrochemical synthesis of metal nanoparticles. *Russ. Chem. Rev.* 87 (11), 1080.
- Yedurkar, S., Maurya, C., Mahanwar, P., 2016. Biosynthesis of zinc oxide nanoparticles using ixora coccinea leaf extract—a green approach. *Open J. Synthesis Theory Appl.* 5 (1), 1–14.